A New Response Approximation Model of the Quadrant Detector Using the Optimized BP Neural Network

Qian Li, Jiabin Wu, Yunshan Chen, Jingyuan Wang, Shijie Gao, and Zhiyong Wu, *Member, IEEE*

***Abstract*—In this paper, a new response approximation model for quadrant detector is proposed based on a BP Neural Network by employing different training algorithms. A total of 1001 data points are gathered to train and test the proposed network. Through optimal configuration, the network with 1 hidden layer and 8 hidden neurons with Log-sigmoid transfer functions in the hidden layer is determined to have the optimum performance. Furthermore, Levenberg-Marquardt (LM) is the best train algorithm while in this case the model is more precise than others. Besides, it shows a good ability to suppress the non-uniformity. The results of experiment reveal that the root mean square error using this model is about 1/5 of that using Fusion method when the beam radius is 0.75*mm*. Meanwhile, its maximum errors under different radii are all less than 6 × 10^{-3}*mm*. Therefore, the new model would have a good application prospect in beam position measurements.**

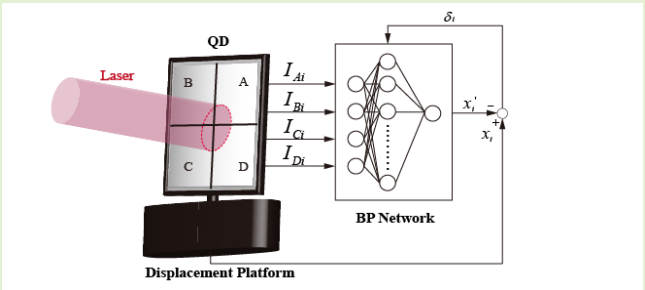

***Index Terms*—Neural Network, optical tweezers, quadrant detector.**

I. Introduction

OPTICAL tweezers is a powerful tool for capturing micron-sized particles suspended in solution by creating optical traps from the laser beam [1]. It has a wide array of applications in biological, quantum science and plasmonics [2]–[6]. The displacement of trapped particles is typically detected by using a Charge-Coupled Devices (CCD) camera or Quadrant Detector (QD). Compared with CCD camera, QD has the advantages of high measurement resolution and short response time [7]–[10]. Using a QD allows nanoscale displacement measurements at a rate of tens of kHz. In biological samples, for example, nanometer resolution at bandwidths up to 100 kHz can reveal details of macromolecular motion [11].

However, the problem with such an implementation is that there is a non-linear relationship between the QD output signal and the centroid position of the beam [12]. The fitting method is a good option to solve this problem. The commonly used normalized central method is actually a first-order polynomial fitting method which is simple and easy to use, but it suffers a low accuracy when the beam center is far from the QD origin. The high-order polynomial fitting method effectively improves the accuracy. However the consequent increase in computation limits its application [13]. Our previous works [14] indicate that the errors of the Infinite Integral Method (IIM) [15] and the Boltzmann method [16], [17] can cancel each other out, and the proposed Fusion method achieves a high accuracy with fewer parameters. Nevertheless, the degree of accuracy of the Fusion method is relatively fixed. Moreover, the non-uniformity of the photoelectric response seriously affects the measurement accuracy.

Machine Learning (ML) and Artificial Neural Network (ANN) are characterized by strong generalization, fast computation speed and nonlinearity, have emerged increasingly in recent decades [18], [19]. In particular, the Back-Propagation (BP) Neural Network proposed by Rumelhart and McClelland [20] is successfully used in pattern recognition, predicting, optimizing decision, enhancing process control [21]–[24].

Manuscript received December 9, 2019; revised December 22, 2019; accepted December 26, 2019. Date of publication December 30, 2019; date of current version March 17, 2020. This work was supported in part by the National Natural Science Foundation of China (NSFC) under Grant 51605465. The associate editor coordinating the review of this article and approving it for publication was Dr. Marco J. Da Silva. *(Corresponding author: Zhiyong Wu.)*

Qian Li is with the Changchun Institute of Optics, Fine Mechanics and Physics, Chinese Academy of Sciences, Changchun 130033, China, and also with the University of Chinese Academy of Sciences, Beijing 100049, China (e-mail: liqian615@mails.ucas.edu.cn).

Jiabin Wu, Yunshan Chen, Jingyuan Wang, Shijie Gao, and Zhiyong Wu are with the Changchun Institute of Optics, Fine Mechanics and Physics, Chinese Academy of Sciences, Changchun 130033, China (e-mail: wujiabin777@163.com; yiyunsn@163.com; wangjy_ciomp@163.com; yoursjohn@163.com; wuzy@ciomp.ac.cn).

Digital Object Identifier 10.1109/JSEN.2019.2963050

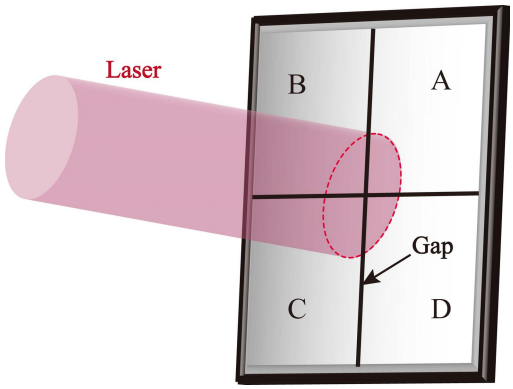

Fig. 1. Beam incident into a QD.

A. Salmanpour et al. used it to deal with this non-linear relationship of QD [25], but there was no specific discussion on network optimization.

In this study, based on the BP Neural Network, a new response approximation model for QD is proposed. A variety of training algorithms are applied, such as Levenberg-Marquardt (LM), Scaled Conjugate Gradient (SCG), Bayesian Regulation backpropagation (BR), and Resilient Back-Propagation (RP). Besides, different transfer functions including Error function (erf), Tan-Sigmoid (tansig), Log-Sigmoid (logsig), Radial basis (radbas), Hard-limit (hardlim), Triangular basis (tribas) and Softmax transfer function (softmax) are deployed in hidden layer and their effects on network precision is estimated. Simulations and experiments are deployed for validation.

II. Conventional Fitting Methods

The QD can be seen as a device consisting of four identical photodiodes separated by small gaps without photoelectric effect [26], as shown in Figure 1.

If there is an incident beam, each quadrant will output the corresponding photocurrent $I_{Ai}, I_{Bi}, I_{Ci}, I_{Di}$. The power intensity distribution of the Gaussian beams is:

$$D(x, y) = \frac{K^2 \exp\left(-2\frac{(x-x_0)^2+(y-y_0)^2}{\omega^2}\right)}{\omega^2}, \tag{1}$$

where ω is the radius of the beam, (x_0, y_0) is the centroid position of the beam [27], then:

$$I_i \propto \iint_{S_i} D(x, y)dxdy (i = A, B, C, D). \tag{2}$$

If the beam radius is much smaller than the detector, the conventional formula to estimate the beam position in x direction is:

$$E_X = \frac{\int_{-\infty}^{\infty}\int_{0}^{\infty} D(x, y)dxdy - \int_{-\infty}^{\infty}\int_{-\infty}^{0} D(x, y)dxdy}{\int_{-\infty}^{\infty}\int_{-\infty}^{\infty} D(x, y)dxdy}, \tag{3}$$

where E_X is the normalized centroid position, representing the extent of deviation from the origin of the QD. However, it is not equal to the centroid position of the beam.

Since:

$$\int_{-\infty}^{\infty} D(x, y)dy = K^2 \exp(-\frac{2(x-x_0)^2}{\omega^2}). \tag{4}$$

Then:

$$E_X = \frac{\int_0^{\infty} K^2 \exp(-\frac{2(x-x_0)^2}{\omega^2})dx - \int_{-\infty}^{0} K^2 \exp(-\frac{2(x-x_0)^2}{\omega^2})dx}{\frac{K^2\pi}{2}}$$

$$= erf(\frac{\sqrt{2}x_0}{\omega}). \tag{5}$$

It can be seen that the y-axis factors (yandy_0) disappear during the above derivation. Since the shape of the QD and the beam profiles are symmetric, it is expected to achieve the same position measurement results in y direction. Consequently, only the position measurement results in the x direction are discussed here. Nevertheless, the problem is that the relationship between E_X and x_0 is a transcendental equation that cannot be solved analytically [28].

A solution for solving this problem is the fitting method. The normalized central method (NCM) is a first-order polynomial fitting method. NCM is a convenient and simple method. However, the error increases sharply when the beam deviates from the origin.

The accuracy of high-order polynomial fitting method often depends on its order:

$$x_0 = \sum_{i=0}^{n} a_n E_X^n. \tag{6}$$

where a_n is the coefficients of polynomial fitting.

Nevertheless, the higher accuracy is often accompanied by a sharp increase in computation, which hinders its application.

Our previous work indicates that the errors of the IIM and the Boltzmann method can cancel each other out, and the proposed Fusion method achieves a high accuracy with fewer parameters:

$$x_0 \approx m * \frac{erf^{-1}(E_X)}{\sqrt{2}} * k_1 + (1-m) * k_2 * \ln\left(\frac{1+E_X}{1-E_X}\right), \tag{7}$$

where, N sets of calculated data are used to find the minimum residual errors. k_1 and k_2 are obtained as:

$$k_1 = \frac{\sum_{n=1}^{N} f_1(E_{X_n}) * x_{1n}}{\sum_{n=1}^{N} f_1^2(E_{X_n})}, \quad f_1(E_X) = \frac{erf^{-1}(E_X)}{\sqrt{2}}, \tag{8}$$

$$k_2 = \frac{\sum_{n=1}^{N} f_2(E_{X_n}) * x_{2n}}{\sum_{n=1}^{N} f_2^2(E_{X_n})}, \quad f_2(E_X) = \ln\left(\frac{1+E_X}{1-E_X}\right). \tag{9}$$

As shown in the Fig.2, when ω is 0.75mm, even the accuracy of the Fusion method is still not enough for optical tweezers whose accuracy needs to reach the nanoscale.

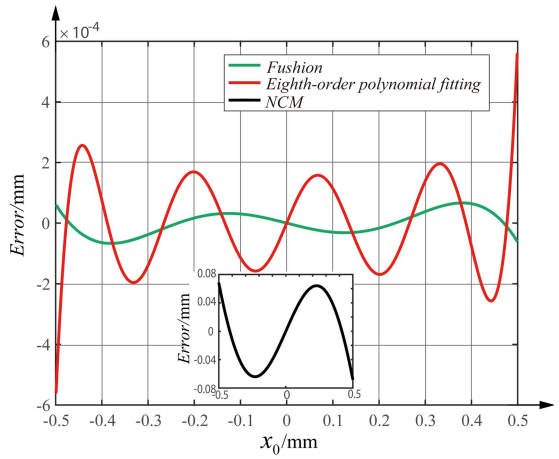

Fig. 2. The simulation curves of positioning errors using three different methods.

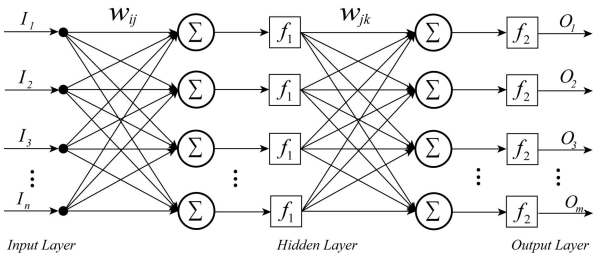

Fig. 3. The architecture of a three-layer back propagation neural network.

III. Methodology

A. Back Propagation Network

Compared to conventional methods, Artificial Neural Network (ANN) has many unique features: Information is stored in the form of the state of each neuron and the interconnections between them. That is to say, distributed storage of information is realized. Since the information storage and calculation process of ANNs are an organic whole, the calculation of it belongs to parallel computing which is more suitable for modern computers. Last but not least, ANNs exhibit high self-adaptability to the environment and a self-learning ability, where the weights on each layer are plastic which can be trained via learning.

Among different kinds of ANN, BP Neural Network is the most reputable, which uses a back-propagation training algorithm. These kinds of ANNs structures in which data move in a forward direction have hidden layer(s) including computational nodes named hidden neurons. In order to increase the performance of the network to have a higher order of accuracy, one or more hidden layers could be added. A three-layer BP Neural Network is shown in the Fig. 3.

The output of the hidden layer is:

$$p_j = f_1\left(\sum_{i=1}^{n} w_{ij} I_i - b_j\right) \quad j = 1, 2...l, \tag{10}$$

where n is the number of input nodes.

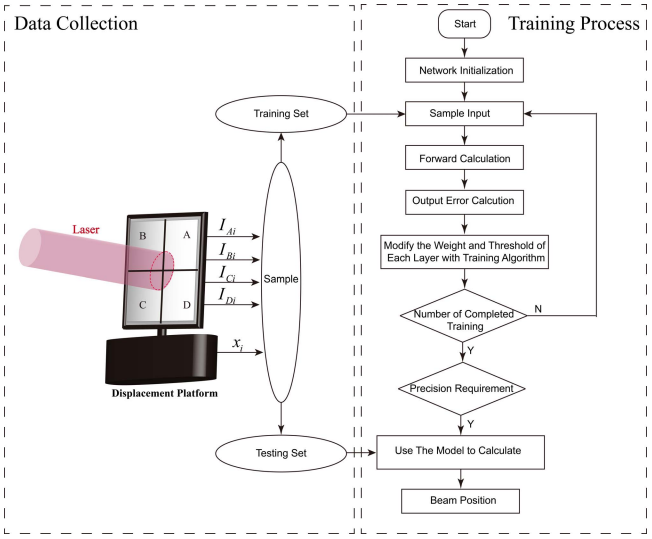

Fig. 4. The scheme of new model.

The output of the output layer is:

$$O_k = f_2\left(\sum_{j=1}^{l} p^{k+1}(i) w_{jk} - b_k\right). \quad k = 1, 2...m. \tag{11}$$

B. ANN Optimal Configuration

The optimal configuration of an ANN can be determined by the number of layers, number of neurons in each layer, training algorithm and the transfer function.

1) Training Algorithm: The scheme is designed as shown in Fig. 4: A beam with a radius of $0.75mm$ is assumed to be incident on a QD with a radius of $1.5mm$ and a gap width of $0.045mm$. The QD is installed on one dimensional displacement platform to achieve precise movement in x direction from $-0.5mm$ to $0.5mm$ at an interval of $0.001mm$. The centroid position of beam x_i and the output current value of each quadrant $I_{Ai}, I_{Bi}, I_{Ci}, I_{Di}$ are recorded. In this way, 1001 simulation data points are collected and divided into training sets (501 points) and testing sets (500 points). When the error satisfies the requirement, the training process ends, and the trained model is evaluated by the testing set.

In this study, the Neural Network Toolbox™ of MathWorks MATLAB® is used to develop the proposed BP Neural Network. Besides, among different available learning algorithms, SCG, LM, BR, and RP are employed to obtain the relationships between the inputs and the outputs.

In order to better evaluate the new estimation model, the maximum error and the root mean square error are adopted:

$$\delta_{xMAX} = MAX\left(|\delta_i|\right) = MAX\left(\left|x_i - x_i'\right|\right). \tag{12}$$

$$\delta_{xRMSE} = \sqrt{\frac{1}{N}\sum_{i=1}^{N}\delta_i^2} = \sqrt{\frac{1}{N}\sum_{i=1}^{N}(x_i - x_i')^2}. \tag{13}$$

From Table I, it can be inferred that the performance of LM is significantly better than other algorithms [29]. Therefore, we choose it as the training algorithm of our new model.

TABLE I
ERRORS USING DIFFERENT TRAINING ALGORITHMS

Training Algorithm	SCG	LM	BR	RP
δ_{xRMSE}/mm	3.354×10^{-5}	1.120×10^{-7}	8.168×10^{-5}	8.319×10^{-5}
δ_{xMAX}/mm	3.127×10^{-4}	7.546×10^{-7}	4.308×10^{-4}	5.662×10^{-3}

TABLE II
ERRORS USING DIFFERENT TRANSFER FUNCTIONS

	Erf	Tansig	Logsig	Radbas	Hardlim	Tribas
δ_{xRMSE}/mm	1.369×10^{-4}	1.711×10^{-7}	1.352×10^{-7}	2.591×10^{-7}	0.065	0.002
δ_{xMAX}/mm	6.165×10^{-4}	8.309×10^{-7}	8.016×10^{-7}	1.103×10^{-6}	0.202	0.010

2) Transfer Function: Transfer function plays an important role in Neural Network. In order to determine the transfer function which is most suitable for this problem, several commonly used transfer functions are chosen and their efficiency is compared.

It can be seen from Table. II that the network using the Log-sigmoid has the lowest δ_{xRMSE} and the δ_{xMAX}. Therefore, the Log-sigmoid is chosen as the transfer function of our new model.

The Log-sigmoid is given in Eq.14.

$$f(x) = \frac{1}{1 + e^{-x}}. \tag{14}$$

3) Architecture: Although Cybenko points out that a BP Neural Network with a single hidden layer can approximate any nonlinear function [30], there is currently no clear theory guiding the design of network architecture. Therefore, how to choose the number of layers of the network and the number of layer neurons is a hard nut to crack.

In this study, the number of nodes in the input layer is only four, and thus the complexity of the network is also relatively low. Hence, there is no need for more hidden layers and the number of hidden layers is set as one.

A series of networks with one hidden layer and n hidden neurons are constructed. Since the multiplication is the main operation form required by a network, the number of multiplication operations can be regarded as the computation C:

$$C = n^2 + 5n. \tag{15}$$

Generally, there is a better fitting result of network with more hidden neurons. However, the subsequent increase in computation will restrict its application in practical engineering. Thus, the efficiency factor ρ is defined which evaluates a network in an all-round way:

$$\rho = \delta_{xRMSE} \cdot C. \tag{16}$$

The number of neurons is changed from 1 to 20 in the hidden layer, iteratively. From Table III, it can be found that the network with $n = 8$ has the lowest ρ which is adopted by our new model.

TABLE III
EFFICIENCY FACTOR OF NETWORKS WITH DIFFERENT ARCHITECTURES

n	1	2	3	4	5	6
δ_{xRMSE}/mm	0.017549	0.002038	6.47×10^{-5}	4.66×10^{-6}	6.52×10^{-7}	1.47×10^{-7}
C	5	10	15	20	25	30
ρ	0.087747	0.020377	0.000971	9.33×10^{-5}	1.63×10^{-5}	4.42×10^{-6}
n	7	8	9	10	15	20
δ_{xRMSE}/mm	1.88×10^{-7}	7.96×10^{-8}	1.33×10^{-7}	2.86×10^{-7}	7.18×10^{-8}	8.20×10^{-8}
C	35	40	45	50	75	100
ρ	6.58×10^{-6}	3.18×10^{-6}	5.99×10^{-6}	1.43×10^{-5}	3.95×10^{-6}	4.92×10^{-6}

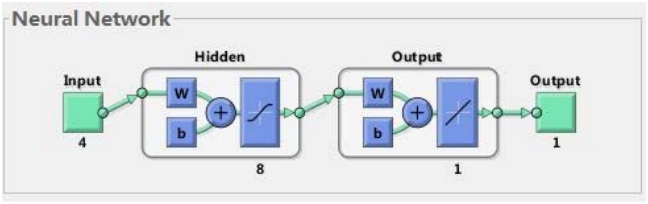

Fig. 5. Model established using NN tool box.

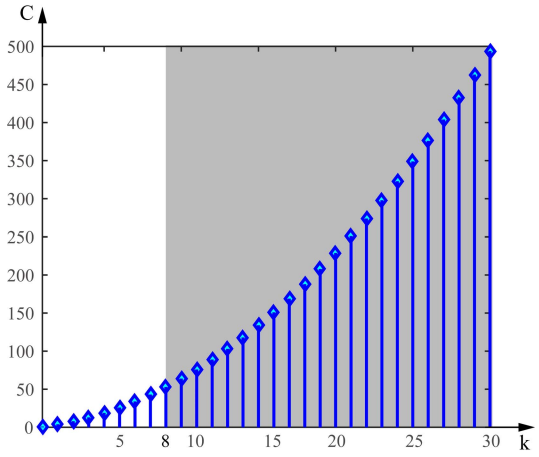

Fig. 6. The computation of the polynomial fitting method with different order. The region is colored gray where computation of the polynomial fitting method exceeds that of our new model.

C. Simulation

After the optimal configuration, the validity of the models is evaluated based on the simulation results.

1) Computation: The computation of the polynomial fitting method increases with its order k, similarly:

$$C = \frac{k^2 + 3k - 2}{2}. \tag{17}$$

As shown in the Fig. 6, when the order reaches to eight, computation of the polynomial fitting method begins to exceed that of our new model. Hence, the eighth-order fitting method is used for comparison in the subsequent simulations.

2) Accuracy: The new model is compared with the Fusion method and the Eighth-order polynomial fitting method, as shown in Fig. 7:

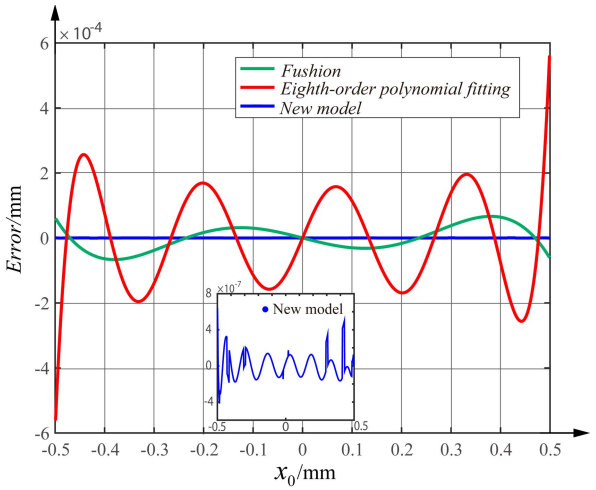

Fig. 7. Comparison of errors between Fusion method, our new model and Eighth-order polynomial fitting method. The insert shows the close-up plot of the new model.

TABLE IV
NUMBER OF PARAMETERS OF OUR NEW MODEL AND THE POLYNOMIAL METHODS UNDER SAME δ_{xRMSE}

ω/mm	polynomial fitting method		our new model	
	δ_{xRMSE}/mm	C	δ_{xRMSE}/mm	C
0.55	2.91×10^{-6}	276	1.56×10^{-6}	40
0.75	1.06×10^{-7}	190	7.88×10^{-8}	40
0.95	6.05×10^{-8}	120	3.58×10^{-8}	40
1.15	3.05×10^{-8}	91	2.80×10^{-8}	40

TABLE V
THE RELATIONSHIP BETWEEN η AND k

η	0.1	0.2	0.3	0.4	0.5	0.6
k	43/39	23/19	49/37	13/9	11/7	29/17

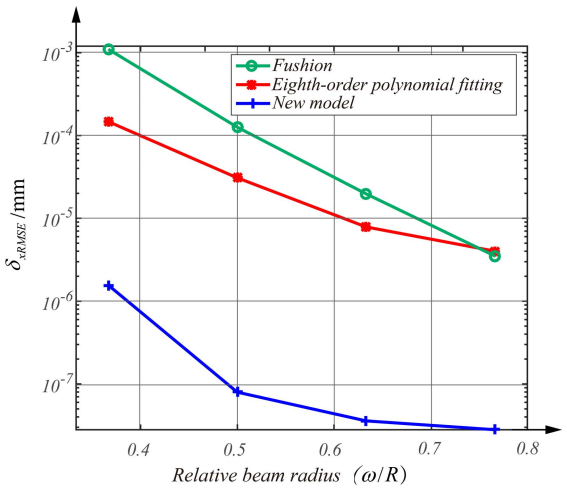

Fig. 8. Comparison of errors between Fusion method, our new model and Eighth-order polynomial fitting method.

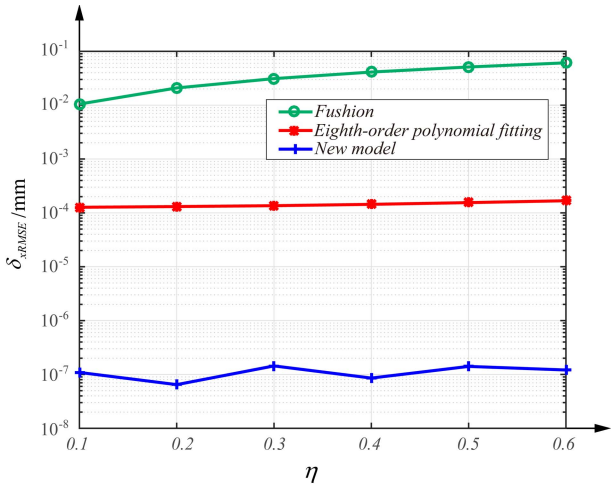

Fig. 9. Comparison of δ_{xRMSE} between the Fusion method, the Eighth-order polynomial fitting method and our new model with different η.

The δ_{xRMSE} of the Fusion method, our new model and Eighth-order polynomial fitting method are $3.103\times10^{-5}mm$, $7.88\times10^{-8}mm$, $1.271\times10^{-4}mm$, respectively. The accuracy of the new model reaches nanoscale which is several orders of magnitude higher than that of the conventional methods.

In order to test the robustness of the new model at different beam radii, the radius of the beam is changed from $0.55mm$ to $1.15\ mm$ and normalized to the relative beam radius [31] (divided by the detector radius R), the simulation results are shown in Fig. 8. It can be seen that the δ_{xRMSE} of our new model which are all less than $1\times10^{-5}mm$ at each beam radius are smaller than that of other methods.

Table IV indicates that the computation required to achieve the same accuracy for a polynomial fit method is larger than that for new model at different beam radii.

3) Non-Uniformity: In the above discussion, the four quadrants of the QD are assumed to have exactly the same responsiveness. In reality, due to the limitations of manufacturing processes and technology, it is well-nigh impossible.

Supposed the working area of the QD is filled with a uniform beam, the output peak signal of each quadrant is v_a, v_b, v_c, v_d. The photo-response non-uniformity index η of the detector is defined as:

$$\eta = \frac{4\max(v_a, v_b, v_c, v_d) - 4\min(v_a, v_b, v_c, v_d)}{v_a + v_b + v_c + v_d}. \quad (18)$$

The non-uniformity of the photoelectric response will seriously affect the measurement accuracy. If we assume that the non-uniformity only exists in the first quadrant, $v_a : v_b : v_c : v_d = k{:}1{:}1{:}1$. The relationship between η and k is shown in Table V.

Considering the non-uniformity, $I_{Ai}, I_{Bi}, I_{Ci}, I_{Di}$ changes to $kI_{Ai}, I_{Bi}, I_{Ci}, I_{Di}$.

As shown in the Fig. 9, it can be seen that as η increases, the accuracy of the Fusion method and the Eighth-order polynomial fitting method decreases. In contrast, our new model is hardly affected which shows high self-adaptability to the environment and a self-learning ability.

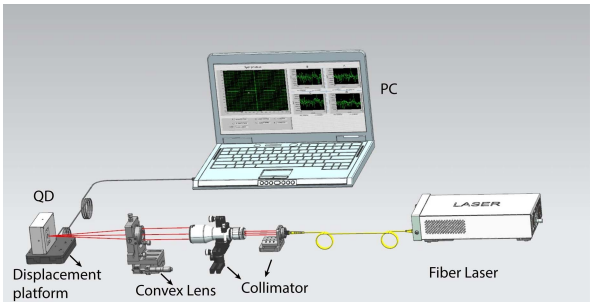

Fig. 10. Measurement system of beam position using the QD.

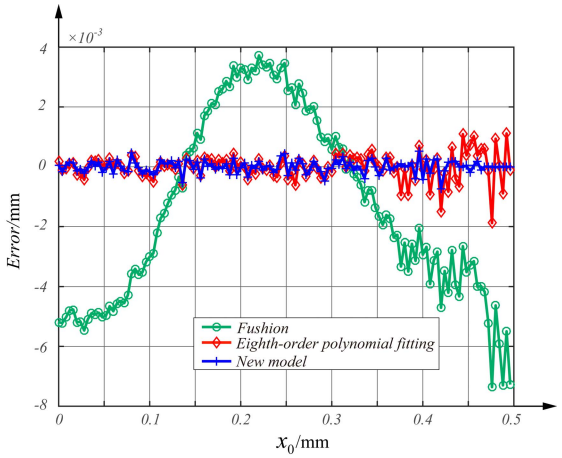

Fig. 11. The positioning error of the new model, the Fusion method and the Eighth-order polynomial fitting method. The measurement range is from 0*mm* to 0.5*mm* for the symmetrical characteristic of beam position errors.

IV. Experiment

A. Experiment Setup

To verify the improvement of the beam position measurement accuracy of our new model, a near-infrared beam position measurement system as shown in Fig. 10 is designed. A 1550 nm fiber-optic semiconductor laser (MDL-1550) with continuously adjustable optical power is used in the experiment system. The Gaussian beams emitted by the laser are changed into parallel beams by collimating and shaping lens groups, and then focused on the QD (FCI-InGaAs-Q3000, 1.5 mm detector radius and 0.045 mm gap) by coupling lens. QD is installed on one dimensional Nano-precision displacement platform (N-644.3A). The signal of QD is amplified, collected by an 18-bit, 400ksps, low noise 4-channel ADC (LTC2344-18) for consistent and real-time data acquisition and then transmitted to the FPGA(Cyclone 4 EP4CE75) for processing.

B. Results and Analysis

Firstly, the radius of the incident beam is adjusted to $0.75mm$, the beam center is shifted from $-0.5mm$ to $0.5mm$ with intervals of $0.001mm$, 1001 experiment data points are collected and divided into training and testing sets. Fig. 11 presents the errors of the three different methods. The δ_{xMAX} of our new model is $5.33\times10^{-4}mm$, which is 92.8% lower than that of the Fusion method ($7.36\times10^{-3}mm$) and 71.7% lower than that of the Eighth-order polynomial fitting method ($1.88\times10^{-3}mm$). Moreover, the δ_{xRMSE} of our new model is $1.48\times10^{-4}mm$ which is about 1/20 of that of the Fusion method ($2.95\times10^{-3}mm$) and 1/2 of that of that of Eighth-order polynomial fitting method ($3.08\times10^{-4}mm$).

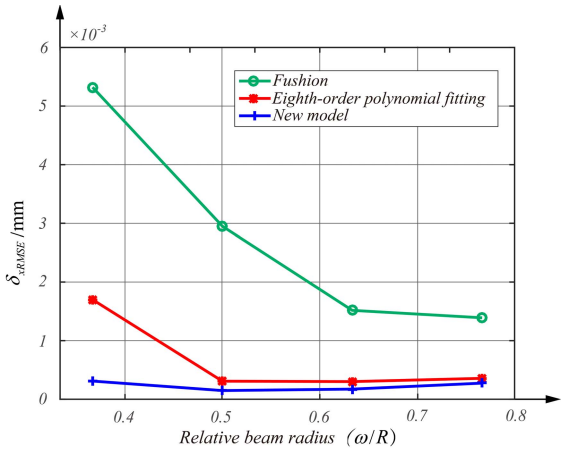

Fig. 12. The δ_{xRMSE} of three methods at different relative beam radii.

TABLE VI
Comparison of δ_{xMAX} of the Conventional Methods and the New Model at Different Radii

Method	ω/mm			
	0.55	0.75	0.95	1.15
Fusion	$1.36\times10^{-2}mm$	$7.36\times10^{-3}mm$	$4.42\times10^{-3}mm$	$3.79\times10^{-3}mm$
Eighth-order polynomial fitting	$4.95\times10^{-3}mm$	$1.88\times10^{-3}mm$	$1.44\times10^{-3}mm$	$1.70\times10^{-3}mm$
New model	$1.97\times10^{-3}mm$	$5.33\times10^{-4}mm$	$7.60\times10^{-4}mm$	$1.10\times10^{-3}mm$

In order to verify the applicability of the new model at different radii, we change the radius from $0.55mm$ to $1.15mm$ and repeat the above steps.

As shown in Fig. 12, the accuracy of our new model which is higher than the Fusion method and the Eighth-order polynomial fitting method shows stability at varying radii. The δ_{xRMSE} of our new model at different relative beam radii are all less than $3\times10^{-4}mm$.

Table VI compares the δ_{xMAX} of three methods under different beam radii. Among the three methods, our new model has the smallest δ_{xMAX} which is less than $2\times10^{-3}mm$ under different beam radii.

Through the above discussion, it can be seen that there is a difference between the experimental results and the simulation results, which is mainly due to the environmental noise. This issue will be the content of our follow-up study. Despite this, the new model presented in this paper shows better accuracy both in δ_{xRMSE} and δ_{xMAX}, and it also exhibits a more stable measurement accuracy for different incident beam radii.

V. Conclusion

The current study has been carried out to investigate the ability of BP Neural Network in dealing with the non-linear

relationship of QD. A total of 1001 data points were gathered to train and test the proposed network. Various training algorithms and transfer functions were applied and their effects on network precision were estimated. After the optimal configuration, a new response approximation model has been proposed. The simulation results showed that accuracy of the proposed model reached nanoscale, which is more accurate than that of the Fusion method. Meanwhile, its computation is less than that of the polynomial fitting method with the same accuracy. According to the experimental results, the new model has stability and accuracy in both δ_{xRMSE} (all less than $3 \times 10^{-4} mm$) and δ_{xMAX}(all less than $2 \times 10^{-3} mm$) for different beam radii.

ACKNOWLEDGMENT

Q. Li thanks Q. Wang for appreciate discussions about this paper.

REFERENCES

[1] J. L. Killian, F. Ye, and M. D. Wang, "Optical tweezers: A force to be reckoned with," *Cell*, vol. 175, no. 6, pp. 1445–1448, Nov. 2018.
[2] M. R. Griffiths, A. Raudsepp, K. M. Mcgrath, and M. A. K. Williams, "Measuring the interaction between a pair of emulsion droplets using dual-trap optical tweezers," *RSC Adv.*, vol. 6, no. 18, pp. 14538–14546, Jan. 2016.
[3] A. Cooper, J. P. Covey, I. S. Madjarov, S. G. Porsev, M. S. Safronova, and M. Endres, "Alkaline–Earth atoms in optical tweezers," *Phys. Rev. X*, vol. 8, no. 4, Dec. 2018, Art. no. 041055.
[4] C.-Y. Li *et al.*, "Using optical tweezers to construct an upconversion luminescent resonance energy transfer analytical platform," *Sens. Actuators B, Chem.*, vol. 282, pp. 790–797, Mar. 2019.
[5] A. Keloth, O. Anderson, D. Risbridger, and L. Paterson, "Single cell isolation using optical tweezers," *Micromachines*, vol. 9, p. 434, Jun. 2018.
[6] M. Habaza, B. Gilboa, Y. Roichman, and N. T. Shaked, "Tomographic phase microscopy with 180° rotation of live cells in suspension by holographic optical tweezers," *Opt. Lett.*, vol. 40, no. 8, p. 1881, Apr. 2015.
[7] D. Schutze, V. Müller, and G. Heinzel, "Precision absolute measurement and alignment of laser beam direction and position," *Appl. Opt.*, vol. 53, no. 28, pp. 6503–6507, Oct. 2014.
[8] D. Zheng, X. Wang, and F. Tang, "An improved method of angle measurement with a position sensitive detector," *Chin. Opt. Lett.*, vol. 5, no. 7, pp. 403–406, 2007.
[9] V. J. Yallapragada, G. L. Mulay, C. N. Rao, A. P. Ravishankar, and V. G. Achanta, "Direct measurement of the Goos–Hänchen shift using a scanning quadrant detector and a polarization maintaining fiber," *Rev. Sci. Instrum.*, vol. 87, no. 10, Oct. 2016, Art. no. 103109.
[10] J. Zhang, M. A. Itzler, H. Zbinden, and J.-W. Pan, "Advances in InGaAs/InP single-photon detector systems for quantum communication," *Light-Sci. Appl.*, vol. 4, no. e286, pp. 1–13, May 2015.
[11] F. Gittes and C. F. Schmidt, "Interference model for back-focal-plane displacement detection in optical tweezers," *Opt. Lett.*, vol. 23, no. 1, pp. 7–9, Jan. 1998.
[12] L. M. Manojlović, "Quadrant photodetector sensitivity," *Appl. Opt.*, vol. 50, no. 20, pp. 3461–3469, Jul. 2011.
[13] M. Chen, Y. Yang, X. Jia, and H. Gao, "Investigation of positioning algorithm and method for increasing the linear measurement range for four-quadrant detector," *Optik*, vol. 124, no. 24, pp. 6806–6809, Dec. 2013.
[14] J. Wu, Y. Chen, S. Gao, Y. Li, and Z. Wu, "Improved measurement accuracy of spot position on an InGaAs quadrant detector," *Appl. Opt.*, vol. 54, no. 27, pp. 8049–8054, Sep. 2015.
[15] Q. Li, J. Wu, Y. Chen, J. Wang, S. Gao, and Z. Wu, "High precision position measurement method for Laguerre–Gaussian beams using a quadrant detector," *Sensors*, vol. 18, no. 11, p. 4007, Nov. 2018.
[16] L. P. Salles and D. W. De Lima Monteiro, "Designing the response of an optical quad–cell as position–sensitive detector," *IEEE Sensors J.*, vol. 10, no. 2, pp. 286–293, Feb. 2010.
[17] D. W. L. Monteiro, "CMOS-based integrated wavefront sensor," Ph.D. dissertation, Dept. Inf. Technol. Syst., Delft Univ. Technol., Delft, The Netherlands, 2002.
[18] M. I. Jordan and T. M. Mitchell, "Machine learning: Trends, perspectives, and prospects," *Science*, vol. 349, no. 6245, pp. 255–260, Jul. 2015.
[19] Y. LeCun, Y. Bengio, and G. Hinton, "Deep learning," *Nature*, vol. 521, pp. 436–444, May 2015.
[20] D. E. Rumelhart and I. L. McClelland, *Parallel Distributed Processing*, Vol. 1, Cambridge, MA, USA: MIT Press, 1986.
[21] M. Nabipour and P. Keshavarz, "Modeling surface tension of pure refrigerants using feed-forward back-propagation neural networks," *Int. J. Refrig.*, vol. 75, pp. 217–227, Mar. 2017.
[22] H. Ansari, M. Zarei, S. Sabbaghi, and P. Keshavarz, "A new comprehensive model for relative viscosity of various nanofluids using feed-forward back-propagation MLP neural networks," *Int. Commun. Heat Mass Transf.*, vol. 91, pp. 158–164, Feb. 2018.
[23] Z. Ye and M. K. Kim, "Predicting electricity consumption in a building using an optimized back-propagation and Levenberg–Marquardt back-propagation neural network: Case study of a shopping mall in China," *Sustain. Cities Soc.*, vol. 42, pp. 176–183, Oct. 2018.
[24] W. Sun and Y. Wang, "Short-term wind speed forecasting based on fast ensemble empirical mode decomposition, phase space reconstruction, sample entropy and improved back-propagation neural network," *Energy Convers. Manage.*, vol. 157, pp. 1–12, Feb. 2018.
[25] A. Salmanpour and S. M. Nejad, "The performance improvement of the target position determining system in laser tracking based on 4Q detector using neural network world," *Int. J. Electron. Commun. Eng.*, vol. 5, p. 8, Aug. 2011.
[26] B. Schmidt and R. Ross, "Position-sensitive photodetectors made with standard silicon-planar technology," *Sens. Actuators*, vol. 4, pp. 439–446, Jan. 1983.
[27] Y. Panduputra, T. W. Ng, A. Neild, and M. Robinson, "Intensity influence on Gaussian beam laser based measurements using quadrant photodiodes," *Appl. Opt.*, vol. 49, no. 19, pp. 3669–3675, Jul. 2010.
[28] X. Ma, C. Rao, K. Wei, Y. Guo, and X. Rao, "Error analysis of the de-crosstalk algorithm for the multianode-PMT-based quadrant tracking sensor," *Opt. Express*, vol. 20, no. 28, pp. 29185–29195, Dec. 2012.
[29] K. Levenberg, "A method for the solution of certain non-linear problems in leastsquares," *Q. Appl. Math.*, vol. 2, no. 2, pp. 164–168, Jul. 1944.
[30] G. Cybenko, "Approximation by superpositions of a sigmoidal function," *Math. Control Signal*, vol. 2, no. 4, pp. 303–314, Dec. 1989.
[31] G. P. Lemos, M. T. C. Souza, V. F. Muniz, F. S. Torres, and L. P. Salles, "Micrometric displacement measurement using CMOS 0.35 μm technology quad–cell," in *Proc. 1st Int. Symp. Instrum. Syst., Circuits Transducers (INSCIT)*, Aug. 2016, pp. 14–18.

Qian Li received the B.S. degree in electrical engineering and automation engineering from the Harbin Institute of Technology (HIT), Harbin, China, in 2015. He is currently pursuing the Ph.D. degree in circuit and system with the Changchun Institute of Optics, Fine Mechanics and Physics, Chinese Academy of Sciences, China. He mainly engaged in weak signal detection.

Jiabin Wu received the bachelor's degree in applied physics from Jilin University in 2011, and the Ph.D. degree in mechanical and electronic engineering from the Changchun Institute of Optics, Fine Mechanics and Physics, Chinese Academy of Sciences, China, in 2016. His research interests include weak signal processing technology and space laser communication technology.

Yunshan Chen received the bachelor's degree from Northeast Normal University in 2007 and the Ph.D. degree from the Changchun Institute of Optics, Fine Mechanics and Physics, Chinese Academy of Sciences, China, in 2012. He mainly engaged in weak signal processing.

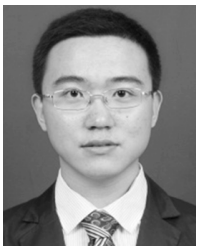

Jingyuan Wang received the bachelor's degree in electronic and information engineering from Jilin University in 2012 and the Ph.D. degree in mechanical and electronic engineering from the Changchun Institute of Optics, Fine Mechanics and Physics, Chinese Academy of Sciences, China, in 2017. His main research directions: electromagnetic compatibility technology and pulse power technology.

Shijie Gao was born in Jilin, China, in 1979. He received the B.E. degree from the Harbin University of Science and Technology, the M.S. and the Ph.D. degrees from the Changchun Institute of Optics, Fine Mechanics and Physics, Chinese Academy of Sciences, China, in 2006 and 2015. From 2006, he has been with the Changchun Institute of Optics, Fine Mechanics, and Physics, Chinese Academy of Sciences, where he is currently a Professor with the Department of Optical-Electronic Detection.

Zhiyong Wu (Member, IEEE) received the bachelor's degree from the Changchun Institute of Optical Precision Machinery, in July 1989. He is a Professor with the Changchun Institute of Optics, Fine Mechanics and Physics, Chinese Academy of Sciences, China. He mainly engaged in the overall technology of optoelectronic measurement and control equipment, and optical fiber communication technology.